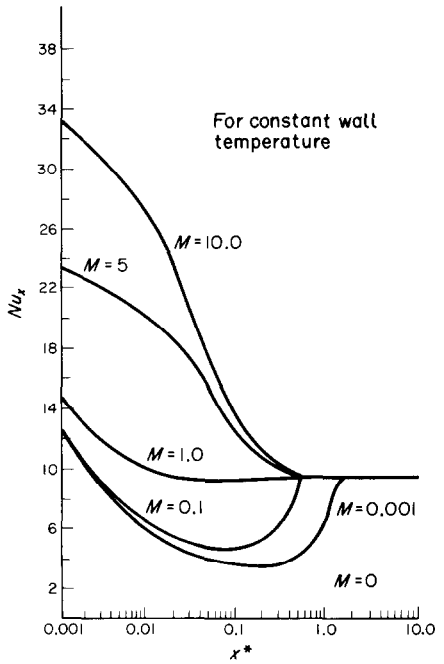

FIG. 1. Variation of local Nusselt number in laminar flow in a tube with viscous dissipation for isothermal boundary condition.

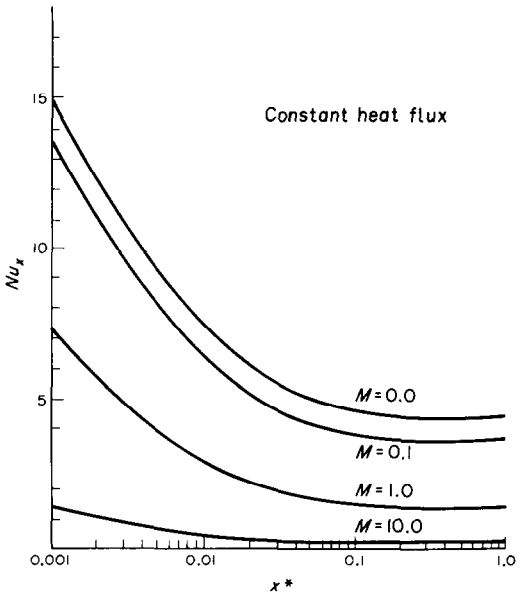

FIG. 2. Variation of local Nusselt number in laminar flow in a tube with viscous dissipation for constant heat flux boundary condition.

Table 3. Eigen values and eigen functions of equations (6) and (9)

Isothermal boundary		Constant heat flux boundary	
λ_n^2	$R_n'(1)$	λ_n^2	$R_n(1)$
7.3136	−1.01430	25.6796	−0.49251
44.6095	1.34924	83.8618	0.39551
113.9210	−1.57231	174.1670	−0.34587
215.2406	1.74600	296.5360	0.31405
348.5640	−1.89085	450.9477	−0.29125
513.7777	2.01450	637.3877	0.27381
711.1111	−2.12594	855.8506	−0.25985

REFERENCES

1. J. R. Sellars, M. Tribus and J. S. Klein, Heat transfer to laminar flow in a round tube or flat conduit, the Graetz problem extended, *Trans. Am. Soc. Mech. Engrs* **78**, 441–448 (1956).
2. H. Nagasue, Steady-state heat transfer with axial conduction in laminar flow in a circular tube with a specified temperature or heat flux wall, *Int. J. Heat Mass Transfer* **24**, 1823–1832 (1981).
3. T. K. Basu, Laminar heat transfer in a tube with viscous dissipation, Master of Engineering Thesis, Calcutta University (1981).
4. R. Siegel, E. M. Sparrow and T. M. Hallman, Steady laminar heat transfer in a circular tube with a prescribed wall heat flux, *Appl. Scient. Res.* **A7**, 386–392 (1958).

Int. J. Heat Mass Transfer. Vol. 28, No. 3, pp. 701–705, 1985
Printed in Great Britain

0017-9310/85 $3.00 + 0.00

Analysis of three-dimensional solidification interface shape

ROBERT SIEGEL
National Aeronautics and Space Administration, Lewis Research Center, Cleveland, OH 44135, U.S.A.

(*Received* 25 *October* 1983 *and in revised form* 18 *June* 1984)

NOMENCLATURE

A_1, A_2 shape coefficients in functions F and G
B_1, B_2 amplitude coefficients in functions F and G
f, g arbitrary functions, $F = f/K$, $G = g/K$
J, M, N, P, R functions defined in equations (9) and (10)
K a constant
k thermal conductivity of solidified material
l half-wavelength of heating variation in y direction, $L = l/w$
n normal to solidification interface, $N = n/w$
q heat flow rate per unit area
t temperature
w half-wavelength of heating variation in x direction
x, y, z Cartesian coordinates, $X = x/w$, $Y = y/w$, $Z = z/w$.

Greek symbols

β, ξ	dummy variables of integration
ϕ	the quantity $k(t-t_w)/wq_{ref}$.

Subscripts

ref	arbitrary reference value
s	at solidification interface
w	at cold wall
0	at the location $X = Y = 0, Z = Z_s$
+	a function of $X+iZ$ or $Y+iZ$.

INTRODUCTION

THE SHAPE of the solidification interface is important in various crystal forming and metal casting processes. The interface is a "free" boundary with a shape that regulates itself to conform to the thermal boundary conditions. One condition is that the interface be at a uniform temperature equal to the solidification temperature. A second condition is that there is convective heat flow to the solid interface from the superheated liquid phase, and this heat flow can be spatially non-uniform. This results in a three-dimensional solidified region that reaches a steady state shape such that the local heating distribution at the interface can be conducted through the solid to a cooled boundary. The final steady state interface shape will be found here; this requires solving a type of inverse problem. The three-dimensional shape of a heat conducting region is to be found that will satisfy steady state conditions at one boundary of both uniform temperature and a specified spatially varying normal temperature derivative.

The background for this type of solidification problem has been given in [1, 2] and will not be repeated here; some related references are in [3–5]. Most of the previous work has considered only two-dimensional situations; relatively little has been done on three-dimensional solutions. For obtaining a solidified shape, a conformal mapping method was used in [1], while in [2] the analysis employed a Cauchy integral method involving some conformal transformations. Since conformal mapping is limited to two dimensions, the three-dimensional problem analyzed here required a different technique. The solutions are generated by continuation into the solid region from conditions at the cooled wall. In addition to showing the behavior of this type of solidification system, the solutions, which are in algebraic form, may be useful for comparisons with those found by numerical methods.

ANALYSIS

The geometry and boundary conditions are shown in Fig. 1. A three-dimensional solidified region is formed on a cold surface kept at uniform temperature t_w that is below the solidification temperature t_s. The thickness of the region $z_s(x, y)$ varies periodically in both the x and y directions as a result of a spatially periodic variation in convective heating $q_s(x, y)$ over the upper boundary of the solid. From symmetry, only the positive quadrant of the upper half plane in Fig. 1 need be considered. Also from symmetry, the four vertical sides of this quadrant all have zero normal temperature derivatives. Hence the analysis also applies to solidification in a rectangular container with four insulated vertical sides and with non-uniform heating at the solidification interface, as supplied by convection from the liquid phase.

Based on some previous work [6], a solution for $t(x, y, z)$ that contains two general real functions f and g is

$$\frac{k(t-t_w)}{wq_{ref}} \equiv \phi(X, Y, Z) = KZ + \frac{1}{2i}\int_{X-iZ}^{X+iZ} f(\cos \pi\xi)\, d\xi + \frac{L}{2i}\int_{(1/L)(Y-iZ)}^{(1/L)(Y+iZ)} g(\cos \pi\beta)\, d\beta \quad (1)$$

where $L = l/w$. This can be adapted here to obtain some three-dimensional solidification interfaces.

When $z = 0$, equation (1) satisfies the boundary condition that $t = t_w$. By taking first derivatives (see equations (3a) and (3b)) it is shown that (1) satisfies the conditions that $\partial t/\partial x = 0$ at $x = 0$ and $x = w$, and $\partial t/\partial y = 0$ at $y = 0$ and $y = l$. Taking second derivatives shows that the Laplace equation

$$\frac{\partial^2 t}{\partial x^2} + \frac{\partial^2 t}{\partial y^2} + \frac{\partial^2 t}{\partial z^2} = 0$$

is satisfied in the region. The remaining conditions to be satisfied are that

$$t = t_s \quad (2a)$$

at the solidification interface $z_s(x, y)$, and

$$k\left.\frac{\partial t}{\partial n}\right|_s = q_s(x, y) \quad (2b)$$

where the spatial variation of q_s is specified. These conditions will be simultaneously satisfied if the proper shape of $z_s(x, y)$ is found.

The first derivatives of equation (1) yield the following relations, where f and g are real functions (i.e. the coefficients in the expressions for f and g are real) of a complex variable

$$\frac{\partial \phi}{\partial X} = \frac{1}{2i}\{f[\cos \pi(X+iZ)] - f[\cos \pi(X-iZ)]\} = \text{Im}\, f[\cos \pi(X+iZ)] \equiv \text{Im}\, f_+ \quad (3a)$$

$$\frac{\partial \phi}{\partial Y} = \frac{L}{2i}\left\{g\left[\cos\frac{\pi}{L}(Y+iZ)\right] - g\left[\cos\frac{\pi}{L}(Y-iZ)\right]\right\}\frac{1}{L} = \text{Im}\, g\left[\cos\frac{\pi}{L}(Y+iZ)\right] \equiv \text{Im}\, g_+ \quad (3b)$$

$$\frac{\partial \phi}{\partial Z} = K + \frac{1}{2i}\{f[\cos \pi(X+iZ)]\, i - f[\cos \pi(X-iZ)](-i)\} + \frac{L}{2i}\left\{g\left[\cos\frac{\pi}{L}(Y+iZ)\right]\frac{i}{L} - g\left[\cos\frac{\pi}{L}(Y-iZ)\right]\left(-\frac{i}{L}\right)\right\} \equiv K + \text{Re}\, f_+ + \text{Re}\, g_+. \quad (3c)$$

Then at the solidification interface

$$\frac{q_s(X, Y)}{q_{ref}} = \frac{k}{q_{ref}}\left.\frac{\partial t}{\partial n}\right|_s = \left.\frac{\partial \phi}{\partial N}\right|_s = \{[(\text{Im}\, f_+)^2 + (\text{Im}\, g_+)^2 + (K + \text{Re}\, f_+ + \text{Re}\, g_+)^2]^{1/2}\}_{Z=} \quad (4)$$

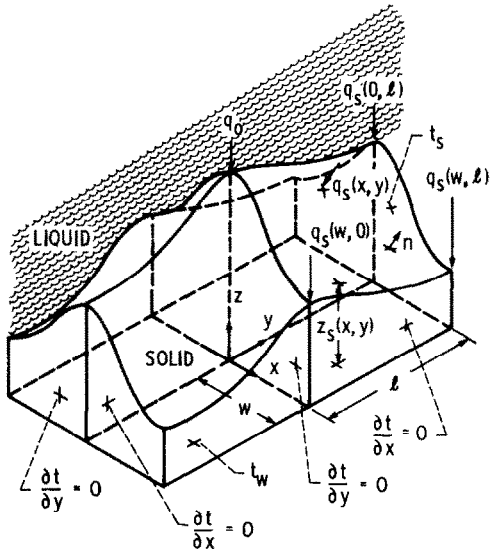

FIG. 1. Solidified region with heat transfer to solidification interface spatially periodic in two directions.

It is convenient to have the dimensionless surface heating distribution along Z_s normalized so that it is equal to unity at $X = Y = 0$. Then with $q_s(X = Y = 0) \equiv q_0$,

$$\frac{q_s(X, Y)}{q_0} = \frac{\{[(\text{Im } F_+)^2 + (\text{Im } G_+)^2 + (1 + \text{Re } F_+ + \text{Re } G_+)^2]^{1/2}\}_{X,Y,Z_s}}{\{[(\text{Im } F_+)^2 + (\text{Im } G_+)^2 + (1 + \text{Re } F_+ + \text{Re } G_+)^2]^{1/2}\}_{0,0,Z_s}} \tag{5}$$

where $F = f/K$ and $G = g/K$. Then equation (1) evaluated at the solidification interface is normalized into the form

$$\frac{k(t_s - t_w)}{wq_0} = \frac{Z_s + \frac{1}{2i}\int_{X-iZ_s}^{X+iZ_s} F(\cos \pi\xi)\, d\xi + \frac{L}{2i}\int_{(1/L)(Y-iZ_s)}^{(1/L)(Y+iZ_s)} G(\cos \pi\beta)\, d\beta}{\{[\text{Im } F_+)^2 + (\text{Im } G_+)^2 + (1 + \text{Re } F_+ \text{Re } G_+)^2]^{1/2}\}_{0,0,Z_s}}. \tag{6}$$

The boundary conditions (2a) and (2b) remain to be satisfied by obtaining the correct Z_s. The quantity $k(t_s - t_w)/wq_0$ on the left side of (6) is a parameter and has the physical significance that when $F = G = 0$, the dimensionless thickness Z_s of the solidified region is uniform and is equal to the value of this parameter (one-dimensional case). When the F and G are not zero, the $Z_s(X, Y)$ distribution obtained from the implicit equation (6) defines a boundary at uniform temperature t_s since the left side of the equation has a fixed value. The $Z_s(X, Y)$ shape depends on the F and G functions, and from equation (5), these functions also provide a heating distribution $q_s(X, Y)/q_0$ at the solidified interface. From equation (3c) the $\partial\phi/\partial Z$ at the base plane $Z = 0$ (the cooled boundary) yields

$$\left.\frac{\partial t}{\partial Z}\right|_{Z=0} \propto 1 + F(\cos \pi X) + G\left(\cos \pi \frac{Y}{L}\right). \tag{7}$$

Hence F and G directly determine the heat flux distribution through the base plane ($Z = 0$) as a function of X and Y. This distribution will be a distortion of the heat flux that passes into the solidification interface, because of the curved three-dimensional heat flow paths through the solidified region. If the functions in equation (7) are chosen with a sufficient number of adjustable degrees of freedom, then the F and G can be modified until the desired $q_s(X, Y)/q_0$ is obtained (to satisfy (2b) within acceptable accuracy) from equation (5) used in conjunction with equation (6) to first find the $Z_s(X, Y)$ values.

The method just described will now be used to obtain some three-dimensional solidification shapes. As an illustrative case, the heating distribution $q_s(X, Y)$, as indicated in Fig. 1, was chosen to vary in a cosine manner in both X and Y

$$\frac{q_s(X, Y)}{q_0} = 1 + \frac{1}{4}\left[\frac{q_s(1, L)}{q_0} - 1\right] \times \left(2 - \cos \pi X - \cos \pi \frac{Y}{L}\right). \tag{8a}$$

The $q_s(1, L)/q_0$ is a parameter, and is the maximum value of the heating distribution; this is reached at the corner $x = w, y = l$ that is farthest from the origin (Fig. 1). At the other two corners the $q_s/q_0 = 1 + \frac{1}{2}\{[q_s(1, L)/q_0] - 1\}$ so that the heating has undergone half of its total increase. In the related work in [1, 2], the two-dimensional shape of a solidified region was found for a cosine heating variation in only one direction by use of two different analytical methods. These results can be obtained using the present method by matching the solution to the following two-dimensional form of the boundary condition (8a) at the interface:

$$\frac{q_s(X)}{q_0} = 1 + \frac{1}{2}\left[\frac{q_s(1)}{q_0} - 1\right](1 - \cos \pi X). \tag{8b}$$

For the cosine heating at the interface given by (8a), the

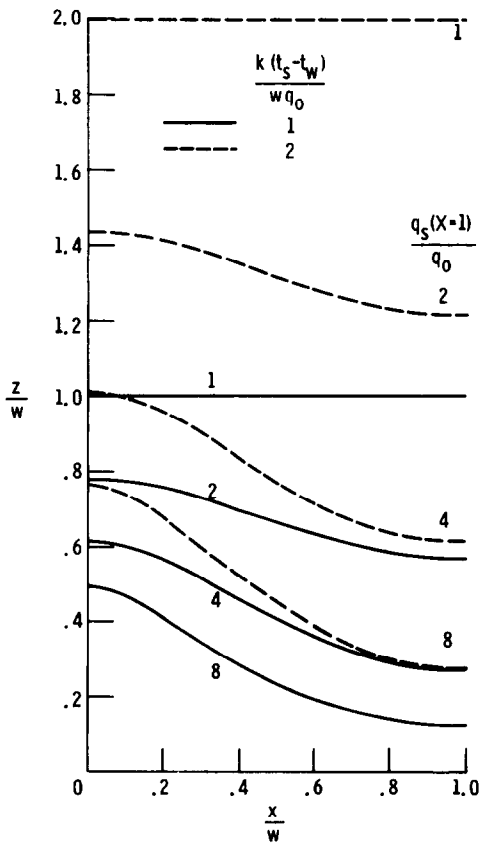

FIG. 2. Two-dimensional free boundary shapes.

Table 1. Amplitude and shape coefficients

(a) Two-dimensional cases

$k(t_s - t_w)/wq_0$	$q_s(X = 1)/q_0$	A_1	B_1
1	1	0	0
1	2	0.064	0.177
1	4	0.196	0.801
1	8	0.288	1.977
2	1	0	0
2	2	0.0084	0.0214
2	4	0.076	0.223
2	8	0.230	0.927

(b) Three-dimensional cases; $k(t_s - t_w)/wq_0 = 1$

L	$q_s(X = 1, Y = L)/q_0$	A_1	B_1	A_2	B_2
1	1	0	0	0	0
1	1.5	0.026	0.0335	0.026	0.0335
1	2	0.055	0.088	0.055	0.088
1	3	0.135	0.235	0.135	0.235
2	1	0	0	0	0
2	1.5	0.021	0.034	0.031	0.114
2	2	0.045	0.090	0.070	0.230
2	3	0.110	0.245	0.180	0.465

functions in equation (7) at $Z = 0$ are expected to be distorted cosine-like functions. The following functions were chosen that will yield this type of shape (the A and B coefficients provide freedom in the adjustment of shape and amplitude):

$$F(X) = J(A_1, B_1, X) \qquad G(Y) = J\left(A_2, B_2, \frac{Y}{L}\right) \tag{9}$$

where

$$J(A, B, \delta) = -\frac{B(1-A)}{2A}\left(1 - \frac{1+A}{1+A\cos\pi\delta}\right).$$

Equation (9) is inserted into equations (6) and (5) to yield

$$\frac{k(t_s - t_w)}{wq_0} = \left\{\frac{1}{1+M[A_1, B_1, Z_s(0,0)]+M[A_2, B_2, Z_s(0,0)/L]}\right\}\left\{Z_s\left[1 - \frac{B_1(1-A_1)}{2A_1} - \frac{B_2(1-A_2)}{2A_2}\right]\right.$$
$$\left. + \frac{B_1}{4\pi A_1}\sqrt{(1-A_1^2)}\ln N(A_1, X, Z_s) + \frac{LB_2}{4\pi A_2}\sqrt{(1-A_2^2)}\ln N\left(A_2, \frac{Y}{L}, \frac{Z_s}{L}\right)\right\} \tag{10a}$$

$$\frac{q_s(X,Y)}{q_0} = \frac{\left\{[P(A_1, B_1, X, Z_s)]^2 + \left[P\left(A_2, B_2, \frac{Y}{L}, \frac{Z_s}{L}\right)\right]^2 + [1 + R(A_1, B_1, X, Z_s) + R(A_2, B_2, Y/L, Z_s/L)]^2\right\}^{1/2}}{|1+M[A_1, B_1, Z_s(0,0)]+M[A_2, B_2, Z_s(0,0)/L]|} \tag{10b}$$

where

$$M(A, B, \eta) = \frac{B(1-A)}{2}\frac{1-\cosh\pi\eta}{1+A\cosh\pi\eta}$$

$$N(A, \delta, \eta) = \frac{\{\sqrt{[1+A)/(1-A)]}(\cos\pi\delta + \cosh\pi\eta) + \sinh\pi\eta\}^2 + \sin^2\pi\delta}{\{\sqrt{[(1+A)/(1-A)]}(\cos\pi\delta + \cosh\pi\eta) - \sinh\pi\eta\}^2 + \sin^2\pi\delta}$$

$$P(A, B, \delta, \eta) = \frac{B(1-A^2)}{2}\frac{\sin\pi\delta\sinh\pi\eta}{1+2A\cos\pi\delta\cosh\pi\eta + A^2(\cosh^2\pi\eta - \sin^2\pi\delta)}$$

$$R(A, B, \delta, \eta) = -\frac{B(1-A)}{2A}\left[1 - \frac{(1+A)(1+A\cos\pi\delta\cosh\pi\eta)}{1+2A\cos\pi\delta\cosh\pi\eta + A^2(\cosh^2\pi\eta - \sin^2\pi\delta)}\right].$$

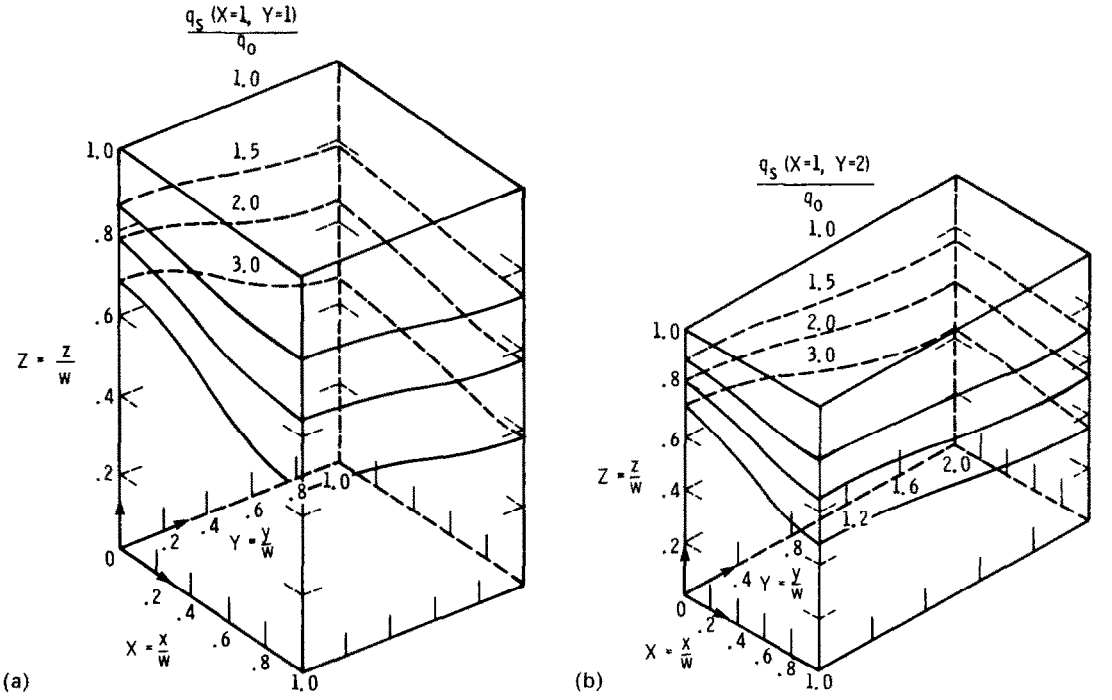

FIG. 3. Three-dimensional free boundary shapes for $k(t_s - t_w)/wq_0 = 1$, (a) square cross-section, $l/w = 1$, (b) rectangular cross-section, $l/w = 2$.

To obtain a free boundary solution a value is selected for each of the parameters, $k(t_s - t_w)/wq_0$, L, and $q_s(1, L)/q_0$. Then the As and Bs are given small values, such as 0.1. Equation (10a) is used at $X = Y = 0$ to obtain $Z_s(0, 0)$ which is then retained in the denominators of (10a) and (10b). Various X and Y are inserted into (10a) and the $Z_s(X, Y)$ are obtained to provide a free surface shape. The corresponding $q_s(X, Y)/q_0$ distribution is then found from (10b). The next step is to adjust the B values to make $q_s(1, L)/q_0$ agree with the specified parameter. This usually takes only a few iterations, and computing times are only in the range of seconds. The shape of the $q_s(X, Y)/q_0$ distribution from (10b) is then compared with

(8a) and adjustments are made in the As and in the B_1 relative to B_2 to improve the agreement. This procedure is continued until the agreement is as close as possible. After obtaining a little experience on how changes in the As and Bs influence the $q_s(X, Y)/q_0$ it was possible to obtain very good agreement with less than 20 trials. The results are discussed in the next section.

RESULTS AND DISCUSSION

By letting the amplitude coefficient B_2 equal zero, the solution in equations (10a) and (10b) reduces to the two-dimensional case and can be compared with results obtained by conformal mapping in [1] and [2]. For each set of parameters $k(t_s-t_w)/wq_0$ and $q_s(X=1)/q_0$, the coefficients A_1 and B_1 were adjusted, as outlined in the Analysis, until the heat flow boundary condition (8b) was satisfied as closely as possible. The factor A_1 gave sufficient freedom in the shape of the F function that the heating boundary condition could be matched very well for all the cases that were selected. The resulting solidification boundaries are shown in Fig. 2. The maximum deviations in matching (8b) occurred for $q_s(X=1)/q_0 = 8$, which is an extreme variation in surface heat flux. In this instance the $q_s(X)/q_0$ curve never deviated from (8b) by more than about 3% of the total amplitude in the heat flux variation, and the solidification shapes in Fig. 2 are estimated to be accurate within a few percent. To verify the method, solidification shapes were first calculated for some of the parameters in [1] and excellent agreement was obtained.

For the two-dimensional solidification interfaces in Fig. 2, the A_1 and B_1 values are in Table 1, part (a). After the A_1 and B_1 were found for a few values of the parameters, it was not difficult to extrapolate to trial values of A_1 and B_1 for other cases. As expected physically, the shapes in Fig. 2 have smaller thicknesses in the regions of high interface heat flux. The thickness variations show the sensitivity of the interface to spatial variations in the convective heat transfer; this is of interest in showing how carefully the convection must be controlled in casting and crystal growing processes requiring that the interface be kept flat. The thickness variations are much less than by assuming locally one-dimensional heat flow through the region; in this instance the local thickness would be in inverse proportion to the heating if the interface is reasonably flat. The two-dimensional heat flow through the region tends to equalize the thickness variations required to accommodate to the nonuniform heat flux at the interface. This also aids the present solution method as the error in predicted thickness is usually much less than the error in matching the heat flow boundary conditions at the interface.

Three-dimensional solidification interfaces are shown in Fig. 3. for a square cross-section and for a rectangle with aspect ratio two. The A and B coefficients are in Table 1, part (b). Since the three-dimensional shape is appreciably more complex than for two dimensions, it is more difficult to match the surface heat flux variation (8a) in all details. Good heat flux matching was obtained for the parameters in Fig. 3; the accuracy decreased for $q_s(1, L)/q_0$ larger than 3, which is a range of rather extreme heat flux variations. The errors in matching the boundary conditions were somewhat less for $L = 2$ than for $L = 1$. It is estimated that for the case with the largest matching errors, $q_s(1, L)/q_0 = 3$ and $L = 1$, the thickness in Fig. 3(a) is about 7% too small in the region of the two corners $X = 1$, $Y = 0$, and $X = 0$, $Y = 1$. Since the results provide the sensitivity of the interface shape to the heating variations, small adjustments could have been made such as increasing the thickness in these corners by several percent, but this was not done for the shapes presented. The thicknesses at the origin $X = Y = 0$ and at the corner farthest from the origin have good accuracy as the interface heat fluxes were matched very well in these regions.

As in the two-dimensional case the local thickness reflects an inverse relation to the interface heat flux. As the $q_s(1, L)/q_0$ is increased, the total energy transferred through the solidified region is increased; hence, there is a decrease in the average region thickness. The examples in Fig. 3 illustrate the three-dimensional solidification shapes that can be evaluated from the analytical solution with very little computing effort.

REFERENCES

1. R. Siegel, Analysis of solidification interface shape resulting from applied sinusoidal heating, *J. Heat Transfer* **104,** 13–18 (1982).
2. R. Siegel and D. J. Sosoka, Cauchy integral method for two-dimensional solidification interface shapes, *Int. J. Heat Mass Transfer* **25,** 975–984 (1982).
3. R. H. Nilson and Y. G. Tsuei, Free boundary problem for the Laplace equation with application to ECM tool design, *J. appl. Mech.* **98,** 54–58 (1976).
4. G. H. Meyer, The method of lines and invariant imbedding for elliptic and parabolic free boundary problems, *SIAM J. Num. Anal.* **18,** 150–164 (1981).
5. J. Crank and T. Ozis, Numerical solution of a free boundary problem by interchanging dependent and independent variables, *J. Inst. Maths Appl.* **26,** 77–85 (1980).
6. R. Siegel and A. Snyder, Analysis of coolant entrance boundary shape of porous region to control cooling along exit boundary, *J. Heat Transfer* **105,** 513–518 (1983).

Int. J. Heat Mass Transfer. Vol. 28, No. 3, pp. 705–714, 1985
Printed in Great Britain

0017-9310/85 $3.00 + 0.00
Pergamon Press Ltd.

Flow patterns of natural convection in horizontal cylindrical annuli

YAN-FEI RAO, YASUTOMI MIKI, KENJI FUKUDA, YASUYUKI TAKATA and SHU HASEGAWA

Department of Nuclear Engineering, Faculty of Engineering, Kyushu University, Fukuoka 812, Japan

(*Received* 26 *March* 1984 *and in revised form* 31 *May* 1984)

NOMENCLATURE

D	diameter
g	gravitational acceleration
k	mesh constant in equation (6)
L	gap width of the annulus, $r_o - r_i$
Nc	number of nodal points in circumferential direction
Nu	mean Nusselt numbers
p	pressure
Pr	Prandtl number, $\mathrm{Pr} = \nu/\alpha$
r	radial distance
R	ratio of the outer to the inner radius, r_o/r_i
Ra	Rayleigh number based on the inner radius r_i, $g\beta(T_i - T_o)r_i^3/\alpha\nu$
Ra_L	Rayleigh number based on the gap width L